# Steep-Dip Seismic Imaging of the Shallow San Andreas Fault Near Parkfield

J. A. Hole,[1*] R. D. Catchings,[2] K. C. St. Clair,[1] M. J. Rymer,[2] D. A. Okaya,[3] B. J. Carney[1†]

**Seismic reflection and refraction images illuminate the San Andreas Fault to a depth of 1 kilometer. The prestack depth-migrated reflection image contains near-vertical reflections aligned with the active fault trace. The fault is vertical in the upper 0.5 kilometer, then dips about 70° to the southwest to at least 1 kilometer subsurface. This dip reconciles the difference between the computed locations of earthquakes and the surface fault trace. The seismic velocity cross section shows strong lateral variations. Relatively low velocity (10 to 30%), high electrical conductivity, and low density indicate a 1-kilometer-wide vertical wedge of porous sediment or fractured rock immediately southwest of the active fault trace.**

Determination of the structure and internal properties, such as geometry, mineralogy, and fluid content, of fault zones is essential to understanding the earthquake process. Exposed faults provide constraints on fault zone properties (*1*), but geophysical imaging is required to determine in situ properties. The San Andreas Fault (SAF) has a 100- to 200-m-wide zone of low seismic velocity identified (but not located at depth) by fault zone–guided waves (*2*, *3*). Other earthquake data only constrain the seismic velocity structure of the SAF on the scale of kilometers. Earthquakes have been well located relative to each other, illuminating fault structure and rupture patterns (*4*–*6*), but have several hundred meters of absolute location error. In comparison, individual faults create a deformation zone up to a few hundred meters wide (*1*), and changes through time create a broader fault zone a few kilometers in width.

Our study region (Fig. 1) has been the site of studies related to the Parkfield Earthquake Prediction Experiment (*7*). A strong lateral contrast in seismic velocity exists across the SAF zone (*8*, *9*) due to juxtaposition of the Franciscan complex, composed of deformed submarine sedimentary rocks, against the Salinian block, composed of granitic and metamorphic rocks. Earthquake data indicate low seismic velocity (*2*, *3*, *8*), high Poisson's ratio (*8*), and seismic anisotropy (*10*) within the fault zone. The earthquakes define a near-vertical plane, but the plane projects to 0.2 to 1.5 km southwest of the active surface trace of the fault (*4*–*6*, *8*, *11*). Electromagnetic data constrain a vertical, ~1-km-wide high-conductivity zone southwest of the SAF, extending from the surface to a depth of 1 to 3 km (*12*, *13*). Drilling through the SAF has been proposed at this site to directly sample mineralogy, stress, and fluids through an earthquake cycle (*14*, *15*).

To date, active near-vertical strike-slip faults have not been imaged as migrated reflectors in seismic reflection sections. Standard seismic reflection acquisition and processing are designed to image reflectors that are close to horizontal. An increase in seismic velocity with depth, which is the usual situation in the upper crust, refracts seismic energy into horizontal ray paths at a range of depths. These refracted rays (both smoothly turning and critically refracted) are the basis of refraction seismology but also are at the correct orientation to be reflected by a steep fault and returned to the surface (Fig. 2A). The large amount of energy refracted by the vertical velocity gradient allows reflections from vertical structures to be as strong as those from horizontal structures (*16*). The

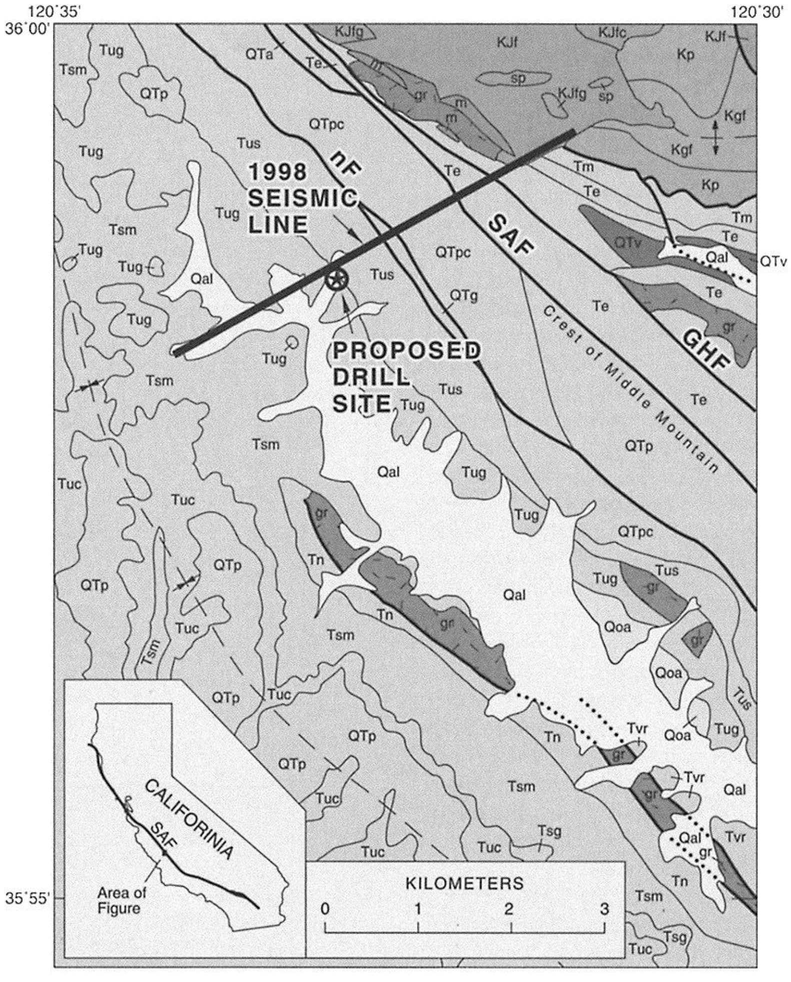


**Fig. 1.** Map of 1998 seismic reflection/refraction line, local geology (*21*), and proposed drill site. The index map shows California and the SAF. Hachured areas labeled gr are granitic Salinian basement southwest of the SAF; K indicates Franciscan complex basement northeast of SAF; T and Q indicate overlying Cenozoic sedimentary rocks.

[1]Department of Geological Sciences, Virginia Tech, Blacksburg, VA 24061–0420, USA. [2]U.S. Geological Survey, MS 977, 345 Middlefield Road, Menlo Park, CA 94025, USA. [3]Department of Earth Sciences, University of Southern California, Los Angeles, CA 90089, USA.

*To whom correspondence should be addressed. E-mail: hole@vt.edu

†Present address: Columbia Natural Resources, 900 Pennsylvania Avenue, Charleston, WV.

petroleum industry has developed techniques to image reflections from the steep sides of salt domes (*17*, *18*). Reflections have been observed from steeply dipping fault planes (*16*), but only Louie (*19*) has attempted to migrate the reflections, a necessary step in determining their subsurface location. Louie's work across the SAF was unable to image the active fault trace.

A seismic survey acquired in 1998, dubbed PSINE (Parkfield Seismic Imaging Ninety-Eight), was designed to produce both refraction and reflection images of the upper 1 km across the SAF and proposed drill site (*20*, *21*). The unusual combination of refraction and reflection survey design is ideal for imaging reflections from steeply dipping structures. Acquisition parameters were 10-m shot and 5-m receiver spacings, 840 channels recording up to 4.9 km offset, and a straight (<20 m variation in 5 km distance) line perpendicular to the fault despite rough topography. Recording the seismic waves to long distances (relative to target depth) allows refraction analysis to constrain seismic velocity to greater depths and allows the recording of steep-dip reflections from greater depths (*22*). Dense sampling allows seismic migration to properly place the reflections in the subsurface image and also directly improves the spatial resolution of the refraction velocity model.

Migration of steeply dipping structures requires an accurate seismic velocity model, which was created by refraction tomography. First-arrival travel times were picked from the data (*23*) and inverted with a nonlinear tomography algorithm (*24*, *25*). The resulting two-dimensional model (Fig. 2A) constrains seismic velocity to about 750 m beneath the surface and has a spatial resolution of about 200 m horizontally and 100 m vertically. The model contains large vertical and lateral variations in velocity (*20*).

Southwest of the SAF, the top of unfractured, unweathered Salinian basement is interpreted to lie at the sharp velocity contrast near the 4.0 km/s contour (Fig. 2A). This surface dips ~10° northeastward to about 700 m depth beneath the proposed drill site and is shallower than the ~1 km depth suggested by previous seismic and electromagnetic studies 3 km to the south (*12*). Overlying rocks with a low velocity gradient (3.0 to 3.4 km/s) between 200 and 700 m depth beneath the drill site may be weathered or fractured Salinian granitic rocks. Alternatively, this depth range may consist of older Cenozoic sedimentary rocks.

The surface trace of the SAF overlies a lateral velocity contrast (Fig. 2A). Relatively low (10 to 30%) velocity persists southwest of the SAF for about 1 km and extends to the base of the model. The southwestern boundary of this zone corresponds with an unnamed fault (nF in Fig. 1). Salinian basement is either absent, too deep, or too deformed to be observed in this 1-km-wide zone. Attempts were made to place higher velocity beneath the deepest rays in this region, but the travel time data do not allow velocity exceeding 4.0 km/s above 1 km depth. Gravity data constrained by the refraction image suggest that Salinian basement is at ~1.2 km depth in this zone (*26*).

The lateral extent of the low-velocity zone corresponds to the observed high electrical conductivity anomaly (*13*). The minimum 1-km basement depth constrained by refraction data and estimated 1.2-km depth from gravity data (*26*) are consistent with the minimum 1.2-km depth for the base of high electrical conductivity (Fig. 3). Exact lateral correspondence and consistency in depth extent suggests a common cause for the low velocity, low density, and high conductivity. The conductivity suggests 10 to 30% porosity filled with saline fluid (*12*), which is consistent with the seismic and gravity models. These rocks could be either a fault-bounded sedimentary basin or a pervasively fractured wide fault zone near the surface.

Kirchhoff prestack depth migration (*19*, *27*, *28*) and the velocity model of Fig. 2A were used to create a seismic reflection image that includes steeply dipping reflectors. The seismic shot gathers were processed before migration to emphasize possible steeply dipping reflections. The data were filtered to relatively low frequencies, and severe mutes were applied to first arrivals, wide-angle reflections, the air wave, and ground roll. This preprocessing eliminated energy from shallow near-horizontal reflections.

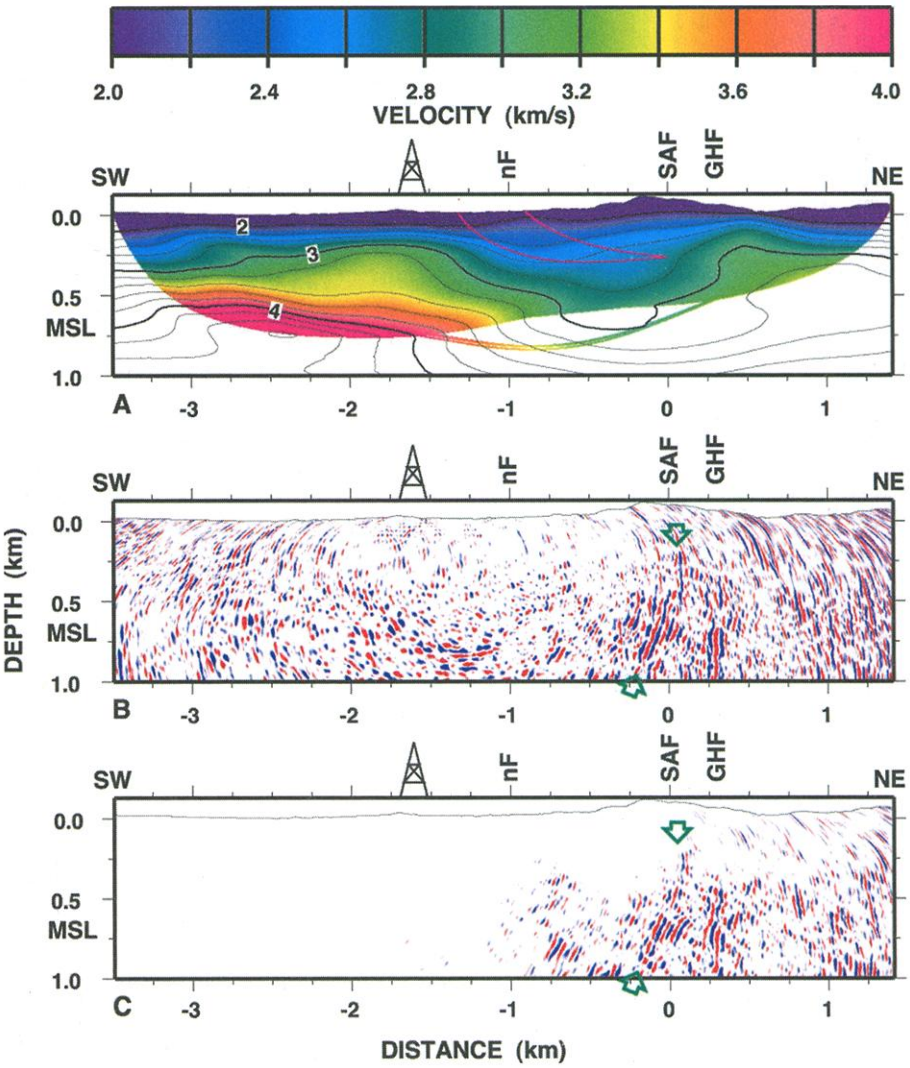


**Fig. 2.** Seismic cross sections across the SAF. The reference datum is 700 m above mean sea level (MSL). **(A)** Seismic velocity model derived from first-arrival travel times (*20*). Contours every 0.2 km/s are labeled in km/s. Areas without rays are white. The magenta line indicates a sample ray path reflected from a vertical plane beneath the surface trace of the SAF. **(B)** Prestack depth-migrated reflection image. Red and blue indicate positive and negative peaks of a reflected wavelet. Green arrows indicate interpreted reflections from the SAF fault plane. Migration artifacts create a circular smile pattern across the image, particularly at the ends of the image. **(C)** Image similar to (B), preprocessed to remove all non–steeply dipping energy in the shot gathers.

The migrated image (Fig. 2B) contains near-vertical features directly beneath the active surface trace of the SAF. These features are interpreted to be reflections from the steep fault plane or narrow fault zone. To test the image, a second migration was performed with different preprocessing. For Fig. 2C, dip filters in the shot and receiver gathers were used to eliminate all energy except that which was horizontally backscattered toward the shot (*16*). The image contains identical steep reflections, confirming that the events are not migration artifacts from shallowly dipping deeper horizons. Figure 2 is the first migrated image of reflections from the near-vertical plane of the active SAF trace, obtained through a combination of careful survey design, accurate velocity model, and appropriate imaging algorithm.

The interpreted SAF reflector is vertical (90° dip) in the upper part of the image but dips 70° to the southwest below about 500 m depth. At 1 km depth, the reflector is ~200 m southwest of the surface trace. Because the velocity model is not sampled by first arrivals beneath ~600 m near the SAF (Fig. 2A), the exact location of the deeper SAF reflector is less well constrained. Using the maximum velocity allowed in this region, a migration was performed that produced the steepest (most vertical) SAF image consistent with the velocity information. In this image, the SAF dips 75° to ~150 m southwest of the surface trace at 1 km depth. The absolute location of the reflector is accurate to within 50 m at 1 km depth and to ~20 m above 500 m depth. The active surface SAF trace is known to within a few meters. The dip of the reflector is accurate to 5°. Beneath 1 km depth, velocity and SAF reflector position are not constrained by the data.

The SAF reflector corresponds with the northeastern margin of the low-velocity zone, suggesting that it bounds this zone. There are suggestions in the data and in some of the migrated images of steeply northeast-dipping reflections that intersect the surface at the unnamed fault (nF) 1.0 km southwest of the SAF (Fig. 1), but we have been unable to produce a satisfactory migrated image of this fault. A vertical reflection is imaged ~300 m northeast of the surface SAF trace below 500 m depth (Fig. 2B). This feature does not extend as close to the surface as the SAF reflection and is thus more difficult to interpret, but it lies directly beneath the northward projection of the Gold Hill Fault (GHF) (Fig. 1).

In central California, earthquakes define a near-vertical SAF plane, but the plane lies hundreds of meters southwest of the surface trace of the fault (*8*, *11*). A systematic error in the velocity model used to locate the earthquakes could account for the apparent offset but would produce a dipping plane more closely aligned with the surface trace (*9*). Improvements in the velocity model have not resolved the discrepancy. Although estimates of absolute horizontal location accuracy for shallow earthquakes are 0.5 to 1.0 km, existing studies place the earthquakes 0.2 to 1.5 km southwest of the surface trace (Fig. 3) (*4–6*, *8*, *9*). Actual misalignment of the surface trace and the deeper fault seems unlikely, because the rocks in the upper 3 km are too weak to generate earthquakes and should break vertically above the stronger deep fault. However, the reflection image suggests that the misalignment is real (Fig. 3). The dipping SAF points to the center of the range of possible earthquake locations at depth. An offset of the surface trace from the deeper stronger fault could be due to strong heterogeneity in the near-surface materials or to changes over geologic time in the location of the active fault.

The SAF reflections, fault to the southwest, low seismic velocity, low density, and high electrical conductivity indicate the complex structure of the shallow SAF. These features are interpreted to be due to a 1-km-wide shallow fault zone consisting of a wedge of sedimentary or fractured rock. The deeper vertical SAF plane lies southwest of the surface fault trace beneath or southwest of this complex surface zone.

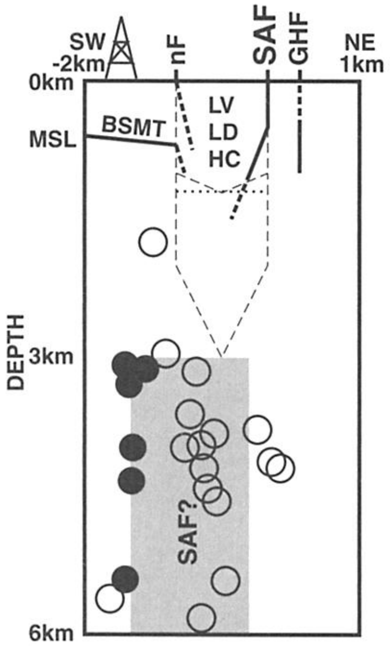


**Fig. 3.** Interpretive cross section across the shallow SAF. Thick lines show sedimentary basement (BSMT), the SAF, the GHF, and an nF as constrained by Fig. 2, dashed where interpreted. The dotted line shows depth to basement near the SAF interpreted from gravity (*26*), consistent with the minimum depth allowed by seismic refraction. Thin dashed lines show the shallowest and deepest possible extent of the high-conductivity (HC) anomaly (*13*); the lateral extent is identical to the zone of low density (LD) and low seismic velocity (LV). Catalog earthquake locations are shown as open circles, and one model of the same earthquakes with better relative locations is shown as overlapping solid circles (*4*). The gray "SAF?" zone indicates the range of other earthquake location models (*4–6*, *8*, *9*), each of which defines a vertical fault.

**References and Notes**


1. F. M. Chester, J. P. Evans, R. L. Biegel, *J. Geophys. Res.* **98**, 771 (1993).
2. Y. Li, P. Leary, K. Aki, P. E. Malin, *Science* **249**, 763 (1990).
3. Y. G. Li, W. L. Ellsworth, C. F. Thurber, P. E. Malin, K. Aki, *Bull. Seismol. Soc. Am.* **87**, 210 (1997).
4. R. Nadeau, T. V. McEvilly, *Bull. Seismol. Soc. Am.* **87**, 1463 (1997).
5. F. Waldhauser, W. L. Ellsworth, *Eos* **80**, F705 (1999).
6. W. Ellsworth, F. Waldhauser, A. Cole, *A New View of the San Andreas Fault: Implications for Earthquake Interaction at Parkfield* (2000) (available at www.ingrm.it/erice/collection.htm).
7. E. Roeloffs, J. Langbein, *Rev. Geophys.* **32**, 315 (1994).
8. A. Michelini, T.V. McEvilly, *Bull. Seismol. Soc. Am.* **81**, 524 (1991).
9. D. Eberhart-Phillips, A. J. Michael, *J. Geophys. Res.* **98**, 15737 (1993).
10. D. Jongmans, P. E. Malin, *Bull. Seismol. Soc. Am.* **85**, 1805 (1995).
11. J. P. Eaton, M. E. O'Neill, J. N. Murdock, *Bull. Seismol. Soc. Am.* **60**, 1151 (1970).
12. M. J. Unsworth, P. E. Malin, G. D. Egbert, J. R. Booker, *Geology* **25**, 359 (1997).
13. M. Unsworth, P. Bedrosian, M. Eisel, G. Egbert, W. Siripunvaraporn, *Geophys. Res. Lett.* **27**, 3021 (2000).
14. S. Hickman, M. D. Zoback, L. Younker, W. Ellsworth, *Eos* **75**, 137 (1994).
15. The SAFOD (San Andreas Fault Observatory at Depth) drilling project, part of the proposed Earthscope initiative (www.earthscope.org/), has been approved by the National Science Foundation but is currently awaiting federal funding.
16. J. A. Hole, H. Thybo, S. L. Klemperer, *Geophys. Res. Lett.* **23**, 237 (1996).
17. D. Hale, N. R. Hill, J. Stefani, *Geophysics* **57**, 1453 (1992).
18. D. W. Ratcliff, S. H. Gray, N. D. Whitmore Jr., *Geophys.Leading Edge* **11**, 15 (1992).
19. J. N. Louie, R. W. Clayton, R. J. Le Bras, *Geophysics* **53**, 176 (1988).
20. R. D. Catchings, M. J. Rymer, M. R. Goldman, J. A. Hole, in preparation.
21. M. J. Rymer *et al.*, in preparation.
22. R. Stadtlander, L. Brown, *Geophysics* **62**, 335 (1997).
23. Supplementary Web material is available on *Science* Online at www.sciencemag.org/cgi/content/full/294/5546/1513/DC1.
24. J. A. Hole, *J. Geophys. Res.* **97**, 6553 (1992).
25. The algorithm (*24*) uses finite differences to compute travel times in a starting velocity model, uses back-projection of the data misfits to update the model, and repeats the process until the data misfit is similar to the picking errors. In order to reduce the effect of the starting model, strong model smoothing was used in early iterations and reduced as the model converged. Resolution and uniqueness were assessed through multiple inversions using different one-dimensional starting velocity models and different smoothing schemes and through tests using similar earth models and synthetic data (*27*).
26. M. S. Miller, M. L. Anderson, R. C. Jachens, C. M. Wentworth, *Eos* **81**, F1217 (2000).
27. B. J. Carney, J. A. Hole, D. A. Okaya, M. G. Imhof, in preparation.
28. The algorithm (*27*) uses finite differences to compute one-way travel times within the velocity model. Based on these times, energy from each seismic trace was assigned to all possible subsurface reflection points, and all traces were summed. Constructive interference produced an image of the reflectors.


29. Data acquisition was funded by the U.S. Geological Survey with assistance from Geometrics Corp. Seismic imaging was funded by a NSF grant to J.A.H. Migration software was developed under an NSF grant to D.A.O. W. Ellsworth, P. Malin, and C. Thurber provided discussion and advice. A. Michael and anonymous reviewers improved the manuscript.

6 August 2001; accepted 19 October 2001